



Research Article

An Extraterrestrial Pt Anomaly during the Late Glacial-Younger Dryas: Viso Massif (Italy and France)

William C. Mahaney^{1,2,*}, Peeter Somelar³ and Allen West⁴

¹Quaternary Surveys, 26 Thornhill Ave., Thornhill, Ontario, L4J 1J4, Canada; ²York University, Department of Geography, 4700 Keele St., North York, Ontario, M3J 1P3, Canada✉; ³Department of Geology, University of Tartu, Ravila 14A, 51014, Tartu, Estonia✉; ⁴Comet Research Group, 2204 Lakewood Drive, Prescott, AZ 86301, USA

*Correspondence to: William C. Mahaney, E-mail: arkose41@gmail.com

Received: 22 May 2024; Revised: 22 May 2024; Accepted: 19 June 2024; Published online: 4 July 2024


How to cite: Mahaney W.C., et al. An Extraterrestrial Pt Anomaly during the Late Glacial-Younger Dryas: Viso Massif (Italy and France). *Airbursts and Cratering Impacts*. 2024 | Volume 2 | Issue 1 | Pages: 1–15 | DOI: 10.14293/ACI.2024.0006

ABSTRACT

Paleosol evidence supporting the Younger Dryas Impact Hypothesis (YDIH) on the Viso Massif of France and Italy is expanded by a Pt anomaly at all sites investigated, accompanied by elevated Os, Ir, Ru, and Rh concentrations at several sites, thus affirming a cosmic driver to the YD climatic shift at 12.8 ka. Original, thin Allerød soils prevalent at the end of the Late Glacial comprise sediments affected by an airburst from a hypothesized secondary daughter fragment or fragments of the main 2P/Encke progenitor comet train that intersected Earth's land surface and its alpine-continental ice sheets. This event has been previously postulated to have breached Lake Agassiz and other proglacial lakes in North America, released meltwater into the Atlantic Ocean through the St. Lawrence and into the Arctic through the Mackenzie River system, after which cold surface water shut down the thermohaline circulation of the Gulf Stream in the North Atlantic. This thermohaline event is the traditional explanation for YD cooling, but was it fast enough to match the pollen evidence, which confirms rapid temperature reversal? Or was an “impact winter” involved? Cosmic signatures reported here include elevated Pt/Pd ratios, Os, Ir, Ru, and Rh concentrations with orders of magnitude (OM) for Ir used to establish the main center of conflagrations that helped trigger an impact winter. While most sections show variable distributions of PGEs, some are fully affected by concentrations entirely through the unweathered substrate or parent material horizons (called “Cu” horizons). Peak distributions of platinum group elements (PGEs) provide new information on the dispersal patterns of grains that add the Western European Alps to the intercontinental array of sites containing the Younger Dryas boundary (YDB) layer, also sometimes called the black mat (BM). Previously, most age determinations for the Alps were derived from relative dating determinations (RD), but here, we report an AMS C14 date from one LG paleosol (G11-Bw) yielding an age of 12,816 ±44 cal yr BP age, coeval with the average 12.8 ka age of the BM.

KEYWORDS

Black Mat-BM, airburst signatures in sand, Pt/Pd ratios, PGEs

© 2024 The Author(s).  This work has been published open access under Creative Commons Attribution License CC BY 4.0 <https://creativecommons.org/licenses/by/4.0/>, which permits unrestricted use, distribution and reproduction in any medium, provided the original work is properly cited. Conditions, terms of use and publishing policy can be found at www.scienceopen.com.

Introduction

The Younger Dryas Impact Hypothesis (YDIH) has been strengthened by recent summaries [1, 2] of linked rinds-paleosols-cosmic airburst signatures in postglacial deposits of the Viso Massif area of France-Italy (Figure 1A, 1B). Combined data of inferred deposit/Allerød soil from proxy Late-Holocene Little Ice Age (LIA) soils provide a base for assessing sediment at time of the Younger Dryas Boundary (YDB), with potential airburst signatures replete in dozens of sites astride the Alps continental divide, all recorded in previous papers [2–10]. These thin, immature Allerød soils at the time of airburst evolved over postglacial and Holocene time into Inceptisols (Cryosols) with nonvarying, almost depth-static (~45 cm) Ah/Bw/Cox/Cu profiles. Within these sections/profiles, cosmic airburst signatures containing variably enriched REEs and base metals are elevated

above crustal averages, with air-quenched grains, melted/welded quartz et al. grains, shocked grains, C- and Fe-rich microspherules, sometimes in chains, fused carbon clusters, Pt metals including Ir, and high Pt/Pd ratios, in paleosols. Weathering rind examples are considered to have been in situ at airburst event-time with instantaneous physical impact and temperature flux (PT forces) affecting rock clasts to ~700 µm depth. The penetration depth of these cosmic forces, albeit measured in only one clast rind, to under ~1 mm depth, most certainly affected post-event weathering fluid penetration through the YD and on into the Holocene. Hence, the post-airburst weathering record can be seen from the ~700 µm depth to rind contact with the clast corestone at ~3 mm. This rind airburst record can be seen and assessed from the SEM image in Fig. 8 in Mahaney [3].

Examples of rinds shown here (Figure 2A–D) from sites G21, G24, G29 and V9 (site G21 not shown in map Figure 1,

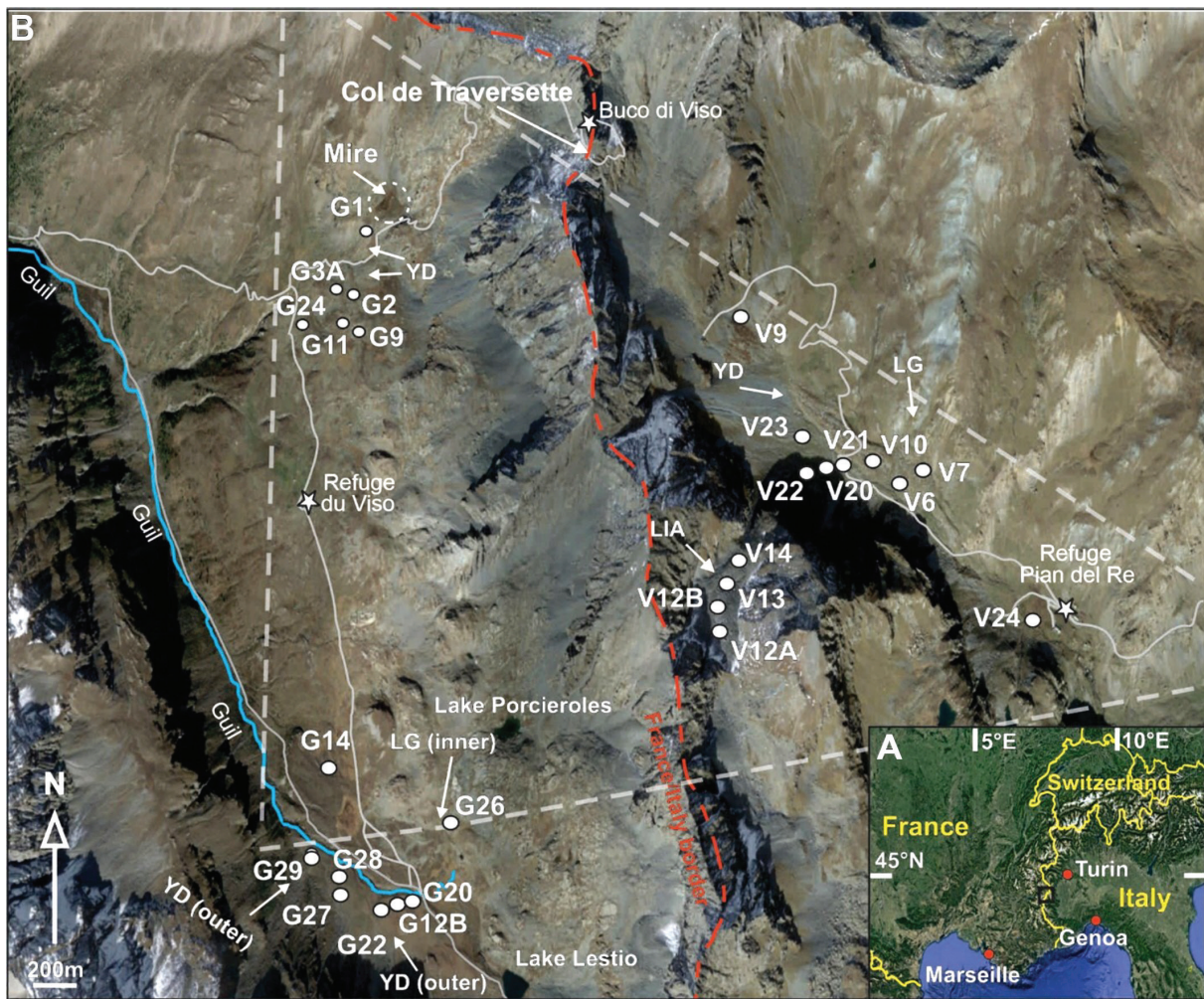


Figure 1: A, Inset map showing the larger area adjacent to the research zone; B, The research area and sites stretch from Guil South (GS) to Guil North (GN) in the upper Guil Valley of France with the upper Po Valley of Italy stretching north and east of Mt Viso (3841 m asl). An approximate isosceles triangle shows the cosmic conflagration area based on sites investigated up to 2017.

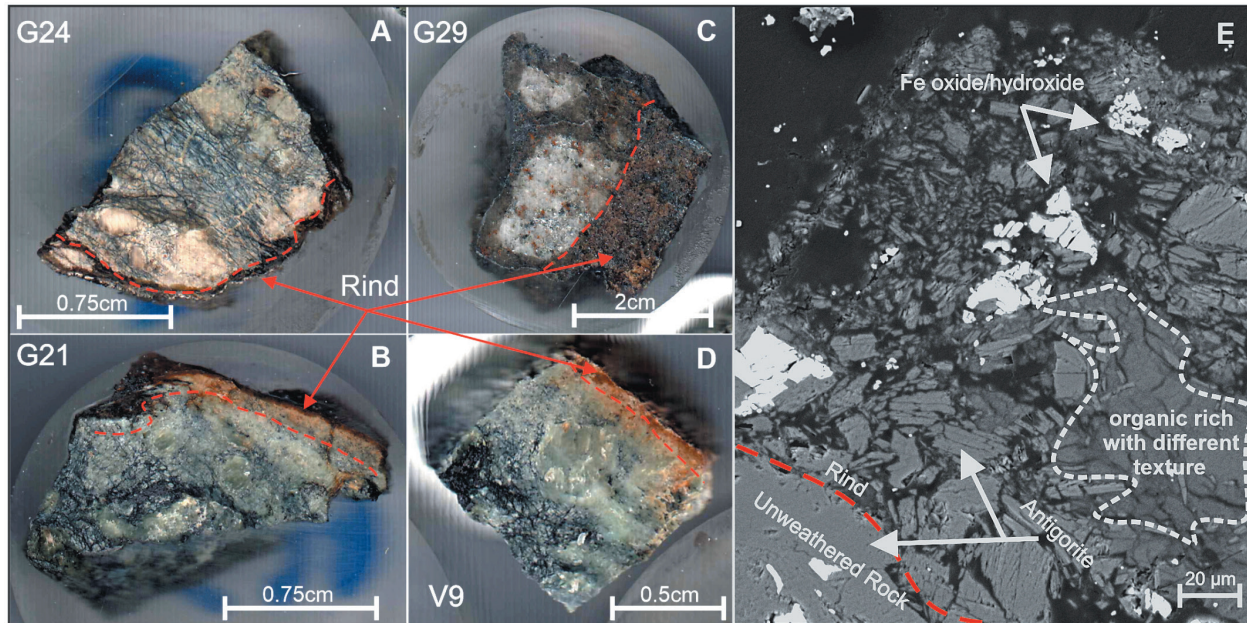


Figure 2: Rind samples. **A**, G24 opaque Fe-carbon encrusted rind (arrow); **B**, G21 Fe-carbon encrusted rind (arrow); **C**, **E**, G29 Fe-carbon encrusted rind (arrow). This rind is 2× thickness of other rinds and is probably reworked into the YD moraine; **D**, V9 Fe-carbon encrusted rind (arrow); **E**, Shattered ~ 160 µm thick rind with a mix of welded grains (arrows), small masses of opaque carbon and shattered grains.

but proximal to G22) are illustrative of rinds recovered from most of the G and V sites documented in Mahaney et al. [1]. In particular, Figs. 6 A, B, and C from Mahaney et al. [1] enlargement shown (in frame 2E) with fused/melted Fe oxide/hydroxide grains, masses of opaque carbon and shattered grains mimic grains analyzed in paleosols cited in the map Figure 1.

Examples of similar grains from Mahaney et al. [1] embedded in paleosols are shown in Figure 3A–C reprinted from Figs. 7 A, B and C in Mahaney et al. [1]. Figure 3A shows an indurated melted/welded mixed-lithology grain from Site V9-Cox, Upper Po valley; B, example of melted-welded fine silts recovered from site G11-Bw, Guil N from Mahaney et al. [9]. This horizon carries an AMS C14 age of $12,816 \pm 44$ (D-AMS 043967); and C, Buckyball-like grain with air-quenched microfeatures in Site G11-Bw, Guil N from Mahaney et al. [9].

Beyond clast rind records, paleosols contain grains with similar archives, minerals dispersed variably horizon-to-horizon, even into the original parent material. The soils affected by the cosmic airburst in early weathering stages probably had profiles similar to A/C/R, A/C/Cu, and C/Cu, for example, with minerals and rinds in the earliest weathering stages as outlined by Mahaney et al. [1]. One of the outstanding physical features of both post-Allerød and post-YD soils, now paleosols, is their depth, which, from research of 75-odd sites, amounts to $\sim 45 \pm 8$ cm. What is more outstanding about this near-uniform paleosol depth in moraines of mixed lithology is the mineral content, ranging from ophiolites, schist-lustres rock, mica-schist, serpentine

group minerals, talc, and gneiss, minerals with variable weathering potential in three major catchments, where postglacial weathering produced widespread near identical Inceptisols. It is also remarkable that this uniform depth occurs independent of minor changes in slope, ground cover, or anthropogenic activity over the last few millennia. Missing in these profiles are the convolutions and ped distortions common with freeze/thaw processes in alpine areas [11]; here, we have well-documented linear boundaries horizon-to-horizon and site-to-site. Given the inordinate thick annual snow accumulations, such may be sufficient to insulate the subsurface from ice crystal growth with frost heave at a minimum.

With the field setting established in brief by Mahaney et al. [1], new PGE distributions in paleosols of the Viso Massif add to the existing YDB or black mat (BM) database, considerably strengthening the YDIH. With Pt metal distributions reported here, we explore affected grain relation to position in the nascent weathering profile, the addition of cosmic-affected allochthonous grains, random movement of affected grains within the recovered profiles, and/or static profiles representing nil movement of affected sediment over time. Given the regional lateral distributions of selected PGEs, at least one airburst occurred over or near the Col de la Traversette (~3000 m asl) (Figure 1B). Networking the affected Viso sites studied so far (Figure 1B, for site location), stretching from Lake Lestio in Guil south (GS) to near the G5 site group to the north (GN), across the continental divide to the V12 site group (2300 m asl), descending into the upper Po valley to 2000 m asl (site V24

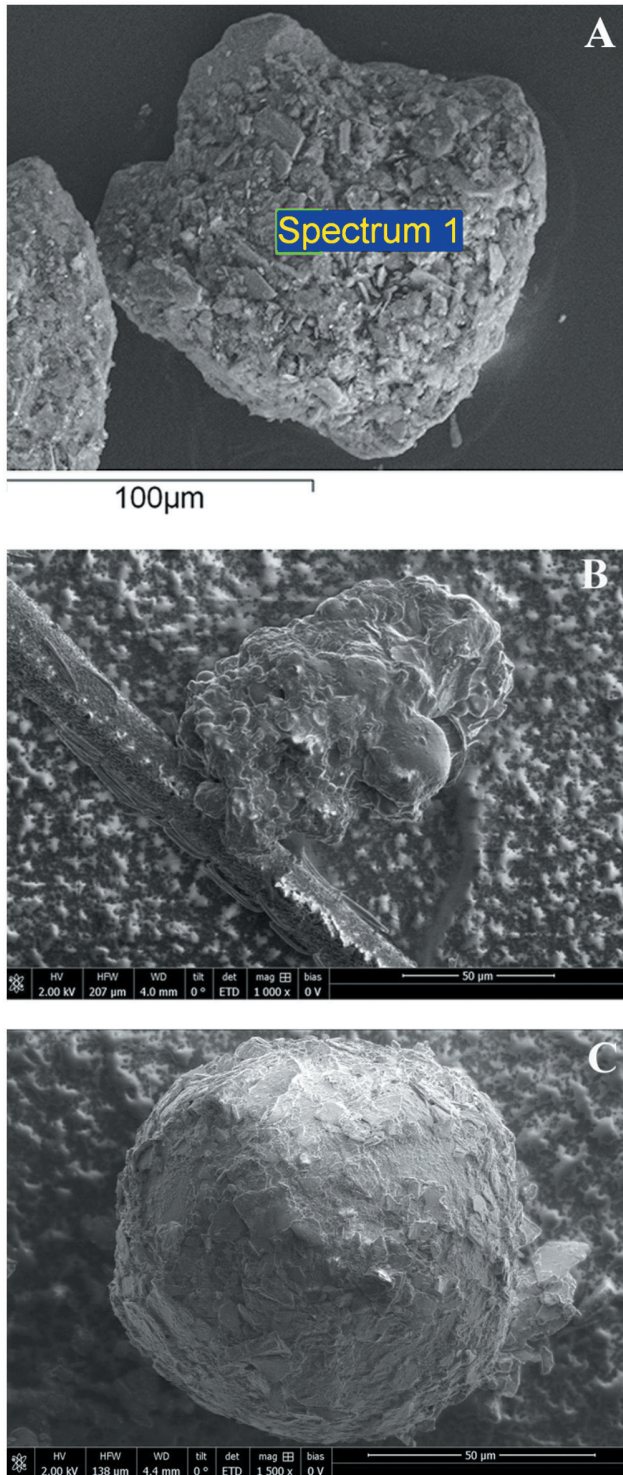


Figure 3: A, Indurated welded mixed lithology of compressed particles from Site V9-Cox, Upper Po valley; B, melted-welded fine silts, Site G11-Bw, Guil N (From [9]); C, Buckyball-like grain with air-quenched microfeatures in Site G11-Bw, Guil N (From [9]).

group of horizons, Figure 1B), thence WSW to G14 comprises a strike area of $\sim 3.3\text{--}3.5\text{ km}^2$ (calculated from Google Earth).

Airburst Model

The hunt for an impact crater related to the 12.8-ka Younger Dryas boundary layer (YDB), often manifesting as the black mat (BM) originator, was highlighted and energized by the discovery in NW Greenland of the Hiawatha Crater. Its discovery resulted from 15 years of research by NASA and subsequent airborne research carried out by the Alfred Wegener Research Institute in Germany [12]. Initially, it exhibited many characteristics strongly suggestive of a very young age and was considered a possible candidate for the YDIH [12–14]. Their diverse evidence for a young Hiawatha includes pristine structure preservation, minor erosion, debris-rich basal ice in situ, unlithified impact sediment in situ, active hydrothermal melting, warm crater, and conformable ice ($\sim 11.7\text{-present}$) underlain by chaotic ice. Subsequent research by Kenny et al. [15] and Hyde et al. [16] pegged the Hiawatha age as Paleocene, slightly younger than the massive 66 Ma Chicxulub Impact in Yucatan [17], essentially disproving any connection between NW Greenland and the intercontinental black mat (BM) sedimentary findings of Firestone et al. [18, 19]. However, most recently, Hyde et al. [20] published dates, obtained from the same sediment samples as previous studies, of $\sim 1\text{Ga}$. This result will mean that sediment washing out of Hiawatha Crater contains grains modified by at least two impact events, likely transported to the crater from far upstream aboard glaciers. While these dating studies per se offer little support for a YDB age, certain aspects—for example, warmth of crater and stratified ice over chaotic ice – keep open the possibility of it being so. The features indicating a young age for the Hiawatha Crater, seemingly incompatible with a Paleocene age, render the postglacial conformable ice column (11.7 ka) over disturbed ice, and other characteristics described above, prime evidence for the elusive YDB impact crater.

The YDIH proposes the intersection of a rogue comet with Earth’s orbit [21, 22], resulting in fragmental airbursts over >60 intercontinental BM sites. Known sites include some along the Laurentide Ice Sheet (LIS) terminal margin [23], in Greenland [24], across to the Scandinavian Ice Sheet, and south to BM sites spread out across North and South America [18, 19, 25, 26], southeastern US, [27], Europe [28], the Middle East [29–32], Africa [33], and Antarctica [34]. Is the 31-km Hiawatha Crater, one-third the size of the Chesapeake Bay Impact and one-eighth of the Chicxulub Crater, possibly consistent with Encke’s intersection of Earth’s orbital plane [21, 22] in terms of producing widespread airbursts and fires, distribution of BM sediment, megafauna extinction, and human (Clovis) displacement. With competing theories between airburst over impact causes, the YDIH is still open given the fact that large-scale impacts are separated by tens of millions of years and reliable dating of Hiawatha by drilling under a km of ice is likely far off in the future. Even if the asteroid struck at the YDB, its size was too small, meltwater/sediment displacement too minimal, and the distance too

great to meet all the accompaniments of the YDIH. Pending a suitable, larger impact find, the Encke airburst model is the best explanation for the YDB.

Major airbursts over the LIS frontal margin are thought to have penetrated deeply enough to melt sufficient ice to add meltwater to the proglacial lakes, including Glacial Lake Agassiz. Drainage from Manitoba through the Great Lakes corridor and into the St. Lawrence, first recognized by Teller et al. [23, 35], was later considered by Lowe et al. [36] to have capped and disrupted the thermohaline Atlantic Current with cold meltwater, sufficient to have generated the YD climatic divide [2]. Such a model – airburst, LIS melt, meltwater release – would have created heterogeneous regional anomalies rather than full-scale, uniform intercontinental atmospheric effects. Other causes, such as increases in CO₂ and CH₄, along with the Dansgaard-Oeschger (D-O) event anomaly in the insolation warming effect underway at the end of the Allerød interstade, have proved deficient to explain the world-widening implementation of the YD climatic anomaly. Combining the original pollen evidence for YD cooling [37–39], LIS melting, and the Thermohaline Atlantic Current model [36] with the comet progenitor cosmic airburst model of Firestone et al. [18, 19] and Moore et al. Part 3 [32] included impact (airburst)-related sites in North and South America, Europe and the Middle East [30–32, 40–44]. These airburst BM sites all have isochronous AMS C14 ages of ~12.8 ka [2, 45, 46], consistent with C14 pollen-affected ages of ~12.7 ka and a more recent AMS C14 age of 12.78 ka [47, 48], updated by Engels et al. [49]. This dating similarity argues for a cause (comet) and effect (pollen) relationship. Thus, it seems the stream of dated sediment leads to a cosmic causal lineage (airburst-melt) to AMS C14 dated BM strata as effect, followed by a sharp upturn in *Dryas* followed by slower overturning of the Atlantic Current. Thus, lacking a designated crater, perhaps the YDIH should be renamed the YDAH, with “A” meaning “airburst.”

Catastrophism/Anti-catastrophism Mindset

Even with cause and effect ironed out, closely fitted by AMS C14 and supported by astronomic pulses of the 2P/Encke Comet [22], pollen-C14 dating of interstadial/YD sites, and BM C14 and RD dated paleosols in moraine and rockfall deposits on the Viso Massif, all abetted with airburst-affected clastic rinds, many workers find it difficult to consider the evidence, relying instead on models which do not tolerate catastrophic events. Ever since the tenets propounded by Sir Charles Lyell in the early 19th century [50], geologists have worked under the umbrella of uniformitarianism that proposes natural processes proceed slowly with catastrophic theories cast aside. Scientists consider uniformitarianism a principal, even astride ever-present earthquakes that are hardly slow, such events later tied to present-day plate theory, which began as continental drift that few accepted, later

acknowledgment of shifting plates that today is a widely acknowledged paradigm.

Beyond this conundrum, critics focus on the experimental physics work carried out to measure nuclear detonations vs cosmic airbursts, showing pressures and temperatures associated with these different explosions to differ by several orders of magnitude. Yet, Bunch et al. [51, 52] compared data from the cosmic sites of Firestone [18, 19] with products from Meteor Crater [53] and Trinity nuclear airburst in Socorro, New Mexico, finding material produced to be morphologically and geochemically similar. Air pressure changes from cosmic airbursts are limited to the ram pressure of fragments, bolides, etc., and resulting temperature changes are governed by an equation of state for air. It was once thought that air pressures from airbursts, controlled by low shock impedance of air relative to sediment/rock, were measured in kPa's, but recent research by Hermes et al. [54] demonstrates that air shock pressures are in the low GPa range. Compare this scenario to Tunguska (1908) [55], where pressure from the ablation of a stony asteroid or comet is estimated at ~100 kPa, which is equal to a 10-12 megaton explosion [56]. Even with this estimated low pressure, the Tunguska airburst produced suspended ice particles at high altitudes, while measurements at Mt. Wilson Observatory showed decreased air temperatures [57]. Although we do not know the exact pressure and temperature exerted by fragmental air burst(s) over the Viso Massif, estimates based on previous research suggest pressures of probably >5 GPa with temperatures >2000 °C [30, 54, 58]. This pressure is sufficient to produce shock metamorphism and melted quartz, which crystallizes from magma at ~650 °C, but pure quartz at one ATM melts at 1700 °C, 1670 °C for B-tridymite, and 1713 °C for B-cristobalite [59].

Regional Area

Using Figure 1B as a base, the PGE field area extends from Lake Lestio (GuilS) to site G5 (GuilN) as a baseline ~0.8 km in the upper Guil Valley, an east segment through site V10, to an apex near V24 in the upper Po valley, a distance of ~1.7 km. The distance V24 WSW to G14 of 1.8 km marks an approximate isosceles triangle with an area of approximately 3-3.5 km². A mixed lithology reduced to its common constituents includes biotite-rich tundra in GS to schistes lustrés (schistose rocks), formerly the bottom of the Tethys Sea along the base to sites G3A and G24, mixed with peridotite and ophiolite ranging to mica schist extending eastward to near V24 at ~2000 m asl [60]. The terrain in this metamorphic area is made up of U-shaped valleys with steep slopes grading up to aretes at various elevations and crossing talus and recessional moraines in places. Figure 1B provides a mosaic of moderate to severe relief.

Despite evidence supporting a catastrophic origin for an intercontinental network of sites with a cosmic signature,

some workers still cling to their uniformitarian beliefs and deny the YDIH.

Materials and Methods

Field analysis

Using 1:20000 air photography, we mapped the field area and selected sites based on nested deposits, all refined during field operations. Random site selection of both post-Allerød and post-YD paleosols yielded depths of <1 m, as required to provide complete sections into the parent substrate (Cu-unweathered deposits). Weathering processes operating over postglacial time produced little change of mineral content but with increasing profile horizonation, despite the wide variation of mineral chemistry and expected variable dissolution. Horizon descriptions follow the NSSC [61], except: **a)** the ‘ox’ designation used with C horizons gave colors that represent the release of secondary oxides/hydroxides (oxihydroxides) as designated by Birkeland [62]; **b)** the ‘Cu’ represents unweathered minerals [63]; and **c)** the Ah horizon designates sediment with organic carbon sufficient to yield colors darker than 10YR 3/1 [64] with colors following the Munsell standard taken from Oyama and Takehara [65]. In most cases, ~300 g samples were recovered from open pits for further lab analysis. Profile schematics are in Mahaney et al. [1] Fig. 4, reproduced here as Figure 4 depicting paleosol G3-3A in upper Guil Valley.

Laboratory analysis

Sediment samples in the lab were first air dried to remove and measure moisture, which allowed determinations of the air-dry equivalent of 50 g oven-dry samples, appropriate wt. of the sample prepared according to ASTM guidelines for particle size analysis. The entire treatment of samples for particle size analysis is in Mahaney et al. [1]. PGEs were analyzed on the < 177-micron fraction of the bulk sample at Activation Laboratories, Ancaster, Ontario, Canada, by ICP, MS, and FA (fire assay). Crustal averages for PGEs are based on Rudnick and Gao [66]. Small pebbles and very coarse sands from G9 and G11, two sites with high concentrations of PGEs, samples with dark coatings were scraped clean with 2-4 g recovered for AMS C14 analysis at Direct AMS Dating Services, Bothwell, Wa., USA. G9 with insufficient wt. of C, no age; G11 with sufficient C produced an age of 12,816 ±44 cal yr BP (D-AMS 043967) age for its Bw horizon, coeval with the average 12.8 ka from Kennett et al. [46].

Results

The sites

Sites were chosen to comprise a mix of LG and YD deposits in the upper Guil (France) and upper Po (Italy) rivers (Figure 1B) to document before (Allerød) and after (YD)-ages of the land surface. The before and after groups straddle the Younger Dryas Boundary (YDB) (12.8 ka), with the before sites affected directly by the cosmic airburst, the

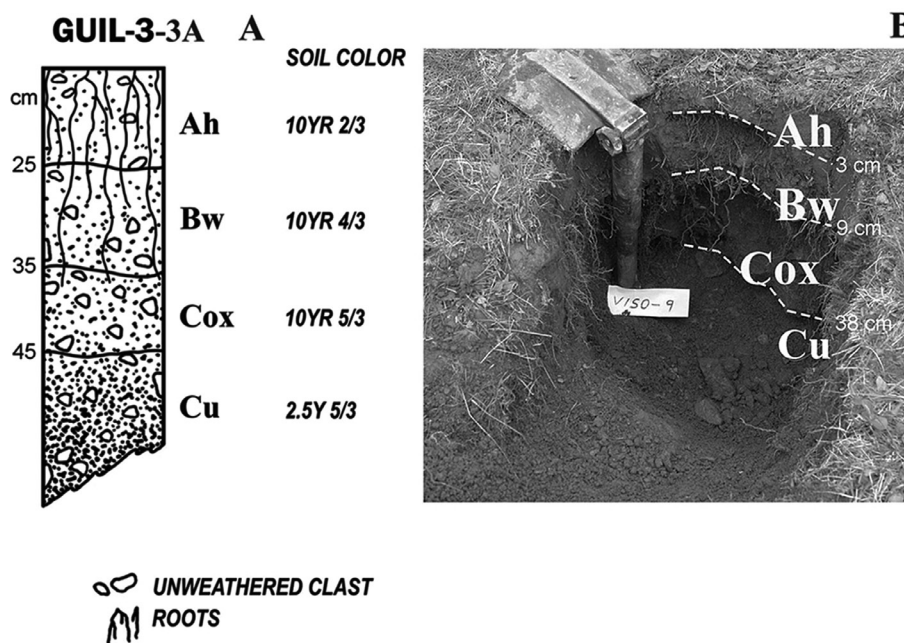


Figure 4: Representative paleosol sections in the Po valley. **A**, Site G3-3A; **B**, Site V9 in LG rockfall debris; All LG-YD paleosols analyzed over the last decade carry similar horizon designations and horizon thicknesses within ±10-15%. Profile thickness varies from 40 to 60 cm with an average of 45 cm; variation of ±15 cm.

after group comprising sediment reworked by advancing YD ice. Of the 70 sites investigated, most comprise deposits in moraine, rockfall, and outwash sediments, the two remaining in a pedostratigraphic sediment stack (V24) comprising a 4-meter thick mass wasted sequence in the upper Po River headwater area at ~2000 m asl. These sites are noted on Figure 1B and comprise: Guil S (G14) and G26); Guil N (G3A, G9, G11, G24); and Upper Po (V9, V12A, 12B, V13, V14, V10, V20A, V22 and V24).

The samples

Samples showing elevated PGE concentrations in paleosols bear little relationship to Cox horizons, which most probably represent part of the original Allerød soil bodies affected by the cosmic airburst. Rather, these paleosol horizons may contain some of the original directly-affected materials which underwent early weathering stages during the mid-Late Allerød, at which point the cosmic airburst occurred. Other cosmic-affected grains are likely from allochthonous origins in the periphery of the blast area close to the continental divide, adjacent south of the Col de la Traversette (~3000 m asl; Figure 1B). Considering that both the LG and YD paleosols contain long-distance daughter products, either directly derived from the airburst or reworked terrestrial materials, all modified by high-temperature-and-pressure weathering, input from aeolian-influx processes, and redistribution within profiles by leaching, soil water movement and sediment compression, it is no wonder element redistribution is

nearly random. Profiles that contain a complete distribution of PGEs, top to bottom of section/profile (i.e., V10) divisions, are probably comprised of directly-affected materials near the center of a fragment (or fragments) airburst detonation.

Pt/Pd ratios

Originally, sites were selected to address questions related to glacial stratigraphy and were later expanded to answer questions related to the YDIH. Major questions center around the elevated Pt/Pd ratio and its relation to PGEs, especially elevated concentrations of Ir.

The Pt/Pd ratio, often used [67] to indicate the presence of other Pt metals, such as Os, Ir, Ru, and Rh, is tested here to determine the correlation between the Pt/Pd ratio and other platinum-group elements (PGEs). In the case of profile V22 (Table 1), the Pt/Pd ratio is highest in the Bw horizon (1.2, tapering off at surface Ah (0.9) and below (Cox (0.7)). In the V9 profile, Pt/Pd registers increasingly positive quotients with depth, from the lowest (0.7) in the Ah to the highest (8.0) in the Cox horizon. Following the presumed correlation between Pt/Pd and PGEs, the correlation is nearly perfect except for Os, which is at detection limits (<2 ppb). Here, the Cox horizon carries the highest concentrations with Ir at 0.4 ppb, well above 2× the order of magnitude (OM) compared to the crustal average concentration [66].

The Pt/Pd ratios for the three horizons in V10 are similar to V22, but with concentrations lowest at the surface (0.8), rising mid-profile to 2.0, and declining below 1.1 in the Cox

Table 1: PGE concentrations^a of sites in the Upper Po Valley, Mt. Viso.

Site	Horizon	Depth (cm)	Os (ppb)	Ir (ppb)	OM ^b	Ru (ppb)	Rh (ppb)	Pt (ppb)	Pd (ppb)	Pt/Pd
^a Crustal Avg.			0.03	0.02		0.34	0.2	0.5	0.5	1.0
Lower Limit			2	0.1		5	0.2	5	2	2.5
YD										
V20	Ah	0-5	<2	<0.1	–	5	20.4	15	4	3.8
V22	Ah	0-5	<2	0.4	2	21	2.3	1.4	1.5	0.9
	Bw	5-25	<2	0.2	1	16	3.3	5.6	4.7	1.2
	Cox	25-37	<2	0.6	3	22	5.8	8.3	11.1	0.7
LG										
V24	Ah	0-5	<2	0.6	3	<5	7.2	1.5	1.8	0.8
	Bw	5-17	<2	<0.1	–	<5	1.3	1.3	1.6	0.8
	Cox	17-29	<2	<0.1	–	<5	6.2	1.0	1.2	0.8
	Bwb	29-40	<2	<0.1	–	<5	4.0	1.3	1.3	1.0
	Coxb1	40-55	<2	0.3	1.5	<5	7.6	1.8	1.2	0.8
	Coxb2	55-59	<2	<0.1	–	<5	2.4	1.2	1.6	0.7
	Cub	59-68	<2	<0.1	–	<5	1.5	1.6	1.8	0.9
V6	Bw	8-25	<2	<0.1	–	<5	27.5	15	3	5.0
V9	Ah	0-3	<2	<0.1	–	<5	3.0	3.5	5.4	0.7
	Bw	3-9	<2	<0.1	–	<5	3.0	1.4	1.1	1.3
	Cox	9-38	<2	0.4	2	5	3.1	7.2	0.9	8.0
V10	Ah	0-6	<2	4.0	20	–	–	1.3	1.6	0.8
V10	Bw	6-20	<2	4.0	20	<5	11.3	1.4	0.7	2.0
V10	Cox	20-46	<2	3.0	15	<5	0.6	1.0	0.9	1.1

^aCrustal averages from Rudnick and Gao [66]. Ir concentration of 0.6 = 3 orders of magnitude above crustal average; Ir conc. of 4.0 = 20 orders of magnitude above the crustal average. Location as follows: V6, 44°42201N, 07°05292E, 2198 m asl; V9, 44°42325N, 07°04974E, 2313 m asl; V10, 44°42294N, 07°05016E, 2290 m asl; V20, 44°42224N, 07°04878E 2278 m asl; V22, 44°49518N, 07°03478E, 2324 m asl; V24, 44°49514N, 07°03489E, 2026 m asl. The Pt/Pd ratios in V22 and V24 are from INAA results from Mahaney et al. [1].

^bOM = Orders of Magnitude for Ir; – = nil.

horizon. If the Pt/Pd ratio suggests an equivalent rollout of Ir, its concentration reaches 4.0 ppb in both the Ah and Bw horizons, dropping to 3.0 ppb in the Cox, a somewhat incongruent relationship. These figures yield orders of magnitude: 20 for the Ah-Bw group and 15 for the Cox. Interestingly, this profile logged the highest soot content of all paleosols sampled on the Viso Massif, and therefore, the site is likely to be close to ground zero of one of the multiple intense YDB airbursts. In contrast, V6 with Pt/Pd of 5 and V20-Ah of 3.8 yield Ir at detection limits, presenting maximum incongruity. Both sites yield Ir concentrations at detection limits of <0.1 ppb.

Enlarging the test from single profiles higher up (2200-2300 m asl) in the local catchments to lower down in the valley, the V24 Section at ~2000 m asl constitutes a pedostratigraphic section of two profiles in mass wasted sediment over glacio-fluvial fill. The ground paleosol in the upper unit overlies the buried paleosol in the lower deposit, which at first observation was considered to belong to LG/YD climatic changes, as confirmed by later analysis. Testing Pt/Pd throughout the section indicates that all horizons are near the detection limit (<1.0). Fire assay analysis showed Os and Ru at detection limits throughout, along with Ir in most samples except the Ah (0.6) and the Coxb1 (0.3) horizons trending positive, 3 and 1.5 OM, respectively. Rh trends with a high-low-high concentration in the ground paleosol, compared with a high to low concentration – Bwb to Cub – horizons in the buried unit. These different trends may represent different leaching histories in the two paleosols related to climate or to vegetation covers. In relation

to the BM, it could be the lower unit formed with increased horizonation under a warming, increasingly postglacial wetter climate, i.e., the Bølling-Allerød, with the original Ab or Ahb horizon truncation occurring with swift release of meltwater, presumably from the airburst heat release. Ultimately, with no Ahb horizon to provide an AMS C14 age, the only recourse to determine the age is from weathering and CIA (Chemical Index of Alteration) value of 63 ([1], Table 7), the latter a nominal index ranging from 1-100, and varying little through the section.

The highest Pt/Pd ratio in the G (Guil) group (Table 2) of samples is 17.7 (G9), with Ir at detection limits and positive numbers for Ru and Rh. Lower Pt/Pd ratios for G3A slowly rose in G11 and G14 but decreased in G24, with values ranging from 0.7 to 23. Ir concentrations range from 3 to 4 (15 to 20 OM) in sites G3A and G11, with concentrations diminished in G14 to 0.9 and 1.6 (4 to 8 OM). Os, if present, is below detection limits. Site G11, horizon Bw, carries an AMS C14 age of $12,816 \pm 44$ (D-AMS 043967), coupled with a Pt/Pd ratio of 26, nil Ru and Rh, but with Ir at 3 ppb (15 OM above crustal average). Similarly, the G11 section carries Ir at 4.0 (ppb) (20 OM greater than crustal average) in the Ah, diminished to 3.0 ppb down-section into the paleosol parent material (Cu horizon at +41 cm depth). The Pt/Pd, following its apogee in the Bw horizon, declines to 5.8 in the Ah, lower still below in the Cox (2.2) and Cu (1.0), whilst the Ir remains steady at 3 overall.

The youngest sample group of Little Ice Age (LIA) age (V12A, B, V13, and V14) (Table 3) produced Pt/Pd ratios of

Table 2: PGE concentrations^a of LG sites in the Upper Guil Valley, France.

Site	Horizon	Depth (cm)	Os (ppb)	Ir (ppb)	OM ^b	Ru (ppb)	Rh (ppb)	Pt (ppb)	Pd (ppb)	Pt/Pd
^a Crust Avg.			0.03	0.02		0.34		0.5	0.5	1.0
Lower Limit			2	0.1		5	0.2	5	2	2.5
G3A	Ah	0-13	<2	4.0	20	–	–	2.1	0.9	2.3
	Bw	13-25	<2	3.0	15	–	–	<0.5	0.7	0.7
	Cox	25-39	<2	3.0	15	–	–	<0.5	0.5	1.0
	Cu	39+	<2	3.0	15	–	–	<0.5	<0.5	1.0
G9	Bw	12-28	<2	<0.1	–	6	15.3	24.8	1.4	17.7
G11	Ah	0-14	<2	4	20	5	20.4	7.6	1.3	5.8
	Bw	14-29	<2	3	15	–	–	15.6	0.6	26
	Cox	29-41	<2	3	15	<5	23.4	2.2	1.0	2.2
	Cu	41+	<2	3	15	–	–	<0.5	1.1	1.0
G14	Ah	0-3	<2	1.0	5	–	–	17.0	1.7	10
	Bw	3-12	<2	0.9	4.5	–	–	8.0	<0.5	16
	Cox	12-34	<2	1.6	8	–	–	10.0	0.7	14
	Cu	34+	<2	1.5	7.5	–	–	35.0	1.5	23
G24	Ah	0-15	<2	–	–	–	–	0.8	0.7	1.1
	Bw	15-36	<2	–	–	–	–	1.4	1.1	1.3
	Cox	36-54	<2	–	–	–	–	2.1	1.6	1.3

Data for G3A and G14 after Mahaney et al. [1]. OM for Ir. Location details as follows: G3A, 44°.42442N, 07°.03171E, 2525 m asl; G9, 44°.42377N, 07°.033259E, 2560 m asl; G11, 44°.42428N, 07°.03189E, 2531 m asl; G14, 44°.41473N, 07°.03536E, 2460 m asl; G24, 44°.42157N, 07°.02827E, 2392 m asl. Some Pt/Pd ratios (G3A and G11) are from Mahaney et al. [1]. Site G24 located adjacent to G24 on inner LG moraine.

^aCrustal average from Rudnick and Gao [66]. – = Insufficient sample.

^bOM = Orders of Magnitude; – = nil.

Table 3: Pt metals of LG age reworked into Neoglacial deposits^a below the Continental Divide. V12A and B are protalus sediments in upper snowpack; V13 and V14 are in Late-Neoglacial moraine above four lower re-energized rock glacier lobes.

Site	Horizon	Depth (cm)	Os (ppb)	Ir (ppb)	OM ^b	Ru (ppb)	Rh (ppb)	Pt (ppb)	Pd (ppb)	Pt/Pd
^a Crust Avg.			0.03	0.02		5	0.2	0.5	0.5	1.0
Lower Limit			2	0.1		5	0.2	5	2	2.5
V12A	C	0-6	<2	0.9	4.5	–	–	4.9	<0.5	9.8
V12B	C	0-8	<2	1.0	5	–	–	0.7	<0.5	1.4
V13	C	0-7	<2	1.5	7.5	–	–	45.7	0.8	57.1
V14	C	0-8	<2	1.0	5	–	–	0.7	0.6	1.2

^aOrders of magnitude (OM) differences shown for Ir. Location and elevation as follows: V12A and V12B, 44°.69736 N, 7°.007382 E, 2784 m asl; V13 44°.69778N, 07°.07585E, 2746 m asl; V14, 44.69809N, 07° 07575E, 2739 m asl. Ice-free cirque, *Coulou di Porco* below the Giacoletti Refuge at 2741 m; lat 44°.696707; 7°. 075935E.

^bOM = Orders of Magnitude.

1.2 to 57.1, the highest in V13 (Figure 1) with Ir topping the sites with a concentration of 1.5 about seven OM, all other sites with values of ~1.0, about 5 OM. These LIA samples contain sediment mass wasted off the continental divide, their Ir content derived distantly from an airburst, followed by later residence following transport into the LIA moraine below the Giacoletti Refuge.

Platinum Group Elements (PGEs)

To further test the Pt/Pd ratio as a predictor of Os, Ir, Ru, and Rh element distributions within profiles, data in Tables 1–3 showed Os consistently below a fire assay detection limit of 2 ppb. Ir, the primary cosmic identifier, is detectable above 0.1 ppb by fire assay and shows variable concentrations ranging from 0.3 to 4 ppb. Compared to the crustal average of 0.02, these Ir values are orders of magnitude (OM) higher, ranging from 1.5 to 20 times. Ru has a lower limit of 5 ppb, variable from 5 to 22 ppb, compared to a crustal average of 0.34 ppb. For comparison, Ru is below detection limits in the Continental Divide samples (Table 3), with a crustal average of 0.34 ppb. Rh, with a lower detection limit of 0.2 ppb and a crustal average of 0.2, varies from 0.6 (0.3 OM) to 27.5 ppb (14 OM). Ru and Rh are sometimes in sync with Ir, as in V10-Bw, V9-Cox, V24-Ah, V24-Coxb1, G11-Ah, and G11-Cox, and sometimes out-of-sync, as in most of the V24 section, V20-Ah and G9-Bw for example. The phrase order of magnitude refers to the smallest power of ten needed to represent a quantity; thus, calculating orders of magnitude and using Ir as the primary guide element, concentrations of 0.5 ppb divided by 0.02 = 25; 25 ÷ 10 = 2.5 OM; 1.0 ppb = 5 OM; 4 ppb = 20 OM. Using OM values provides a direct measure of Ir released by the BM event, and with Tables 1–3, it becomes easy to calculate the near center of the airburst.

Moving on, distributions of Ir and associated PGEs within sections offer various trends that sometimes center on lower horizons (Cox and Cu) as residuum from Allerød soils that suffered directly from the postulated airburst. Using Ir as the main cosmic airburst element, subsoil horizons such as V9-Cox and V22-Cox are two horizons in two sections in particular that fall into this category, with OM ranging from

1.5 to 20, respectively. Both profiles carry lower Ir in surface horizons comprising the Ah-Bw group, postulating post-event loading of allochthonous sediment with lower concentrations. Still, other profiles such as V10 and V22 (Table 1) in the upper Po and G3A and G11 in the upper Guil (Table 2) have OM values of 1 and 20, followed by G14 with values of 4.5–8 OM. Ru and Rh trail Ir with variable concentrations in all these cases, somewhat spectacularly in G9, G11, V9, V10, V20, and V22. Rh in V24-Ah and Coxb1 rises in concert with Ir, falling lower in all other horizons. In all cases, Ir, sometimes in line with Ru and Rh, falls into disjunct or bimodal patterns representing postulated Allerød sediment at the base (Cox), followed upward in section with nil concentrations in Bw horizons (disjunct) or lower concentration (bimodal), thereupon increasing upward to the surface. These patterns – full profile, disjunct, and bimodal – may represent the retention of affected sediment in situ mixed with the later influx of allochthonous materials or a complete variable redistribution of affected sediment by compression or soil water movement.

REEs

With concentrations often correlating with the PGEs, the REEs might be expected to yield higher than crustal average concentrations in both the LREEs and HREEs. Surprisingly, the LREEs (La-Sm) show only 14 samples higher than the crustal average; The HREEs, markedly higher, show 23 samples higher than the crustal average. Summaries of REEs in all samples analyzed can be found in Mahaney et al. [1]. Because some REEs may be taken up as electron receptors by bacteria, some element concentrations may be lower today than at the time of the airburst (12.8 ka). Cerium is remarkable with respect to microbial uptake, thus reducing its concentration, as pointed out by Young et al. [68].

Discussion

Viso (V) group

Sections range from a **bimodal** distribution of Ir in V22 (Table 1) showing high-low-high concentrations surface to

depth to **disjunct** in V9 (nil to higher at depth) and V24 with an indeterminate distribution of positive concentrations in the Ah (0.6 ppb = 3 OM) and Coxb1 (0.3 = 1.5 OM), detection limits elsewhere in the section. Following the Ir distribution, Ru's trend is similar to bimodal occurrences in V22, disjunct in V9, with V24 at detection limits throughout the sequence. Rh presents with positive values for every sample; V22 increases slowly with depth, and V9 is nearly uniform at ~3 ppb (=1.5 OM) throughout the profile. V24 posts a Rh bimodal disposition of 7.2 ppb (=3.6 OM) at the surface, diminishing to 1.3 ppb (0.65 OM), rising with depth in the Cox to a level of 6.2 ppb (=3.1 OM); the Bwb horizon starts at 4.0 ppb (=2 OM), rises to 7.6 (=3.8 OM) in the Coxb1 and diminishes with depth into the Cub horizon. The distributions of PGEs within profiles and profile-to-profile, while predominantly random, show a preference for high concentrations from airfall-influx (V22 and V24) and for transference to lower horizons within coarse sediment sections (V9). Within the profiles, some lower horizons tend to show higher concentrations (V9 and V22), although V10 is an exception.

With PGEs present through profiles, concentrations range from near uniform, as in V10, whereas more often, distributions tend to be disjunct or bimodal. Where disjunct as in V20 or V24, suspicion rests on airfall influx processes redistributing allochthonous grains, i.e., V20-V24-Ah horizons. Distributions down-profile, as in V9 and V24, either relate to affected mineral presence near the surface (V24-Ah) during the airburst event or to grains being redistributed later by soil water movement (V24-Coxb1). The bimodal distribution of Ir in V22 suggests the Cox might profile the airburst event itself, whereas the Ah targets allochthonous additions as the event unfolded. Profile to profile, there is inherent randomness in most profile concentrations, with distributions ranging from near full to disjunct vs. bimodal in both the upper Po and upper Guil profiles.

Guil GS-GN group

Within the G group (Guil Valley), Os remains below detection limits, whereas Ir shows similar downward trends in G3A and G11, with higher concentrations (4 ppb = 20 OM) at the surface, diminishing to 3 ppb (15 OM) in lower horizons. Relative to crustal averages for Ir, this trend registers a slow decrease from surface to depth. G14 presents lower concentrations of Ir that increase from 1 ppb at the surface to 1.5-1.6 ppb at depth, translating into 5 OM at the surface and increasing to 7.5-8 OM at depth. The only data for Ru and Rh are in G9 and G11. Scattered Ru ranges from <5 to 6 ppb in G9 to G11; Rh from ~15 to ~23 ppb between G9 and G11. Thus, the distribution of PGEs may relate to variable and higher-than-expected temperatures at airburst, high enough to boil (3500 °C), vapor produced, cooling rapidly, and condensing on variably distributed sands. Such effects might explain the presence/absence of PGEs in individual samples.

Airburst centers

Major airburst site accumulation centers are reported at sites G3A, G9, G11, G14, and G24, with Ir elemental concentrations up to 20 orders of magnitude above the crustal average. Additionally, V10 is an important site, displaying high soot content and from 1 to 20 OM for Ir concentrations. Ancillary sites V22, V20-Ah, and V6 display concentrations with Ir OM from <0.1 to 3, rising to 20 in site V10. Based on Ir groupings, there may be two major high-pressure-and-temperature centers, possibly representing two separate airbursts or two daughter-caused conflagrations from one airburst. Given the separate sites for which Ir and associated PGE data are available, it is possible to set a baseline from G14-G24-26 to G3A-G9-G11, with a north tangential segment passing through V10 to V24, thereupon extending west-southwest to G14-G24-G26, as presented above in Figure 1. All relevant sites are encompassed within this somewhat aberrant isosceles triangle, with sites subjected to high-pressure-and-temperature waves radiating in different directions. The area covered by the postulated airburst might be larger, requiring an expanded future network of sites.

Whether one or two airbursts detonated over the continental divide, presumably at low altitude, the main force may have been skewed somewhat eastwards inside the Italian Frontier. This assessment is made from the ultra-high Pt/Pd ratios – V12A (9); V13 (~57) – with medium-high Ir concentrations of 1 to ~1.5, 5 to 7.5 OM. Considering the bulk of this measured material survived mass wasting off the divide into the couloir astride the Giacoletti Refuge, some cosmic material must have been lost. Thus, Pt concentrations reported here are considered minimum.

Wider view

As Mahaney [2] pointed out, the collision of Earth with the trail of progenitor comet 2P/Encke produced an airburst 'shower' over much of the world that was not conducive to preserving some large species, as evident with the extinction on several continents of ~35 megafaunal species, including giant sloths, saber-toothed cats, mastodons, and mammoths. Interconnected airbursts with the potential to produce a conflagration causing an impact winter [69, 70], also generated dust plumes capable of reaching the Mesosphere (~500 km altitude), where lack of gravity ensured long preservation of YD cooling, perhaps the most significant climatic divide of the Neogene. The 1.2 kyr YD climatic record preserved in ice cores, lake cores, and fluvial sections is also present in paleosols and clastic weathering rinds, as demonstrated herein. The composition of this record consists of mm to nm size terrestrial and cosmic grains exhibiting dendritic and air-quenched surface morphologies [7], with melted, welded, and spherulitic materials, often comprising opaque carbon masses, regularly found in outer rims of clastic rinds [4]. In most situations, affected materials are found within a thin, 2-3 cm thick black stratum (color = 10YR

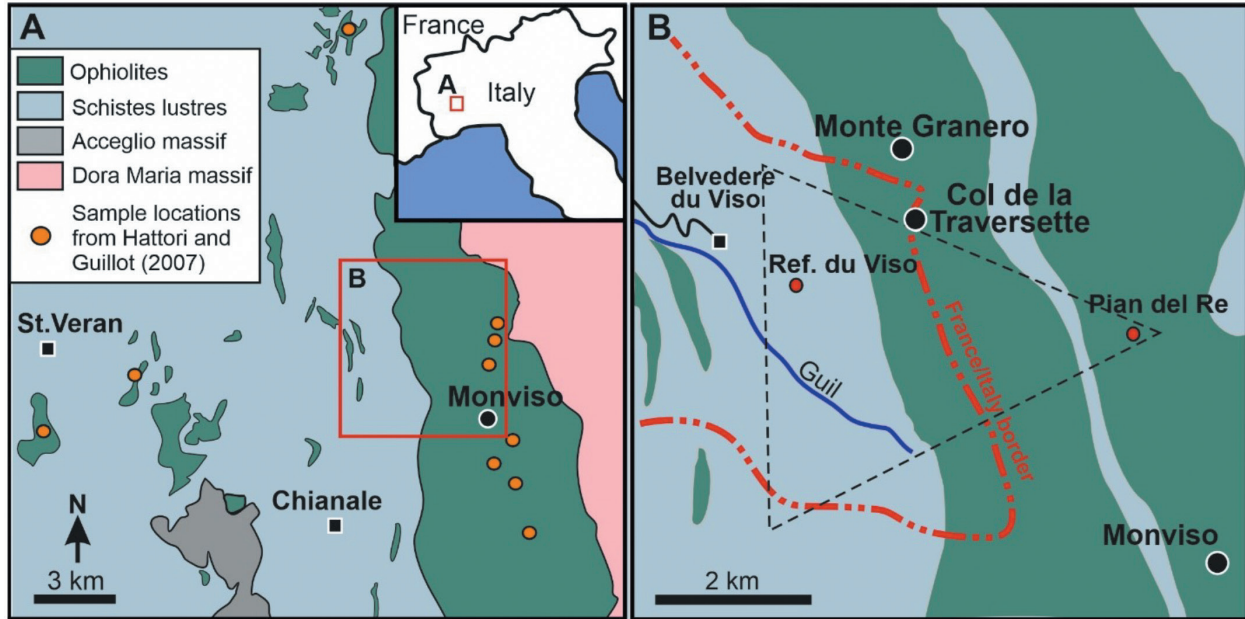


Figure 5: Simplified geological map of the studied area. **A**, Geological map of southwestern Alps modified after Hattori and Guillot [73] showing the distribution of Pt sites (in orange); **B**, Geological map of current study area modified after original Geological Map of France [74]. Approximate isosceles triangle covers paleosol sites discussed within. The inset map shows the area in **A** over the French/Italy continental divide.

1/1), offset from ice or variable colored lacustrine or fluvial sediment, or inset within dark, peaty material, the latter making identification of the BM bed difficult [10]. In other environmental situations, such as paleosols in moraine localities of the Alps [1] and Antarctica [34], impact-affected grains are found mixed with unaffected terrigenous grains added post-event by airfall influx processes. A recent geochemical-petrological study analyzed the spherules produced by an airburst over the East Antarctic mountains from Walnumfjellet in the Sør Rondane Mountains of Queen Maud Land, Antarctica [71, 72]. These particles, dated to 430 ka., closely resemble airburst particles from BT58 in Antarctic Victoria Land, dated between 2.3–2.7 Ma. Both events are considered to result from comet trail/ablating asteroid fragmental airbursts, similarly in line with the BM discussed here, an image of terrestrial destruction and conflagration on a regional to hemispheric scale. Airbursts in the geological record are among the most ephemeral and under-recorded catastrophic geohazards, perhaps far greater than earthquakes or massive tsunami flooding events. This event provides an important case study for defending the Earth, which is under constant threat from asteroids and rogue comets.

Stratigraphically, in the Alps, cosmic grains are found randomly dispersed in: Allerød-age sediment core materials, now full-fledged paleosols; reworked affected sediment of YD push moraine overlying older LG moraine; farther afield in surface horizons of post-MMCO (middle Miocene climatic optimum) moraine in the Dry Valleys of East Antarctica [34]; and clastic rinds in paleosols (Alps).

In all these contexts, identification of BM sediment is difficult, which may explain why so many workers have overlooked relevant cosmic material, thinking that, since they missed BM sediment, such finds must not exist.

Source bedrock from the ancient Tethys Sea contains serpentinites-ophiolites with higher than usual PGE concentrations [73]. However, their site locations (Figure 5) astride the arete north of Mt. Viso contain marginally higher/lower concentrations than some PGE concentrations in paleosols reported here. We hypothesize that some concentrations reported from sites on Figure 1 (overview on Figure 5) differ from PGE distributions reported in 2007. Therefore, our paleosol data add to the total Pt element data pool reported for the Viso Massif, which sums up and supports evidence for a cosmic airburst at the YDB (12.8 ka).

Conclusions

Based on stratigraphically superposed deposits (upper Guil) and LG/YD merged moraines in the upper Po valley, relative dating controls are reinforced by an AMS C14 dated Bw horizon in site G11. The resulting $12,816 \pm 44$ cal yr BP (DAMS-043967) age for G11-Bw dovetails nicely with AMS C14 age control on LG glaciofluvial sediment in the MUM7B site below Pico Mucuñuque (4620 m asl) in the northwestern Andes, which yielded an age of $12,787 \pm 30$ (D-AMS 043968; [2]). Both ages fall within the Bayesian chronological analyses of Kennett et al. [46], consistent

with a synchronous age of 12.8 cal yr BP for the Younger Dryas boundary (BM) on four continents. Correlation of the G11-Bw age with an elevated Pt/Pd ratio and Ir at 15 OM above crustal average strongly support a cosmogenic link to the 2P/Encke comet trail and conflagration of part of the Viso Massif at 12.8 ka. This proposed scenario dovetails nicely with the age summaries of a worldwide synchronous conflagration posited in Wolbach [69, 70, 75].

The randomness of PGE distributions in LG and YD paleosols reflects the randomness of high-pressure-and-temperature waves generated by a cometary fragment or fragments exploding over the massif. Airburst energy melted and vaporized cometary and resident rocky materials in local deposits, generating a giant plume of terrestrial and cometary ejecta, the smallest diameters of which likely reached the upper atmosphere, with intense heat release melting local glaciers. Droplets of molten terrestrial material entrained in the airburst plume would have quickly condensed and solidified, falling back to Earth as sand-silt-sized ejecta particles that would have settled onto area soils and incorporated into paleosols. These ancient markers are hard to find since they formed in layers of rock and soil (now paleosols) that, at inception, would have been mms to cms in thickness. In some cases, coatings on clasts are only tens of micrometers in thickness – only the top 1.5 μm was imaged by SEM at 15 kV. This paper illustrates that these coatings often contain Ir and other PGEs with ppb concentrations. Given the melting point of Pt at 1772 $^{\circ}\text{C}$ and the boiling point at ~ 3600 $^{\circ}\text{C}$, with both dependent on pressure, it is likely the airburst temperature was ~ 2000 $^{\circ}\text{C}$, possibly higher, with Pt randomly distributed, differentially condensing on both terrestrial and cometary materials [29]. Still, other finer grade size materials (<4 μm) might have breached the stratopause, rising into the Mesosphere where the loss of gravity might have maintained them in place to cool the climate for the duration of the YD.

The distribution of PGEs in two significant concentrations (V9, 10, 22 vs. G3A-9-11, 14) supports the possibility of the airburst of one or more cometary fragments over the Continental Divide with high-pressure-and-temperature waves directed downward onto the Guil and Po valleys. Secondly, occurrences in YD deposits appear random, varying from mid-paleosol profile occurrences to Cu horizons comprising mainly unweathered materials, more or less paralleling occurrences on bedrock that reflect preservation dependent upon protection from weathering and erosion. Since paleosol sampling comes from the mid-section of each horizon, Pt occurrences are likely more random in the offset upper and lower quarters of each horizon. In this case, Pt concentrations indicate that the main target area was the continental divide south of the Col de la Traversette, parallel to the upper Po and Guil catchments, declining to the south and lower in both valleys. With elevation, the main affected asymmetrical area lies between ~ 3200 – 2000 m asl.

Acknowledgements

This work was funded by minor research grants awarded during 2002–2022 from York University and the National Geographic Society (Grant no. 9988-16) to WCM. We are indebted to Professor Volli Kalm (deceased-2017, University of Tartu, Estonia) and Max Bezada (UPEL, Caracas) for initial insight into the source/history of the stark black bed in the MUM7B section of the northwestern Andes when initial work on the YD-LG stratigraphy was underway (1996–97). Volli Kalm, former geology faculty and later President of the University of Tartu, was a primary member of the Andean Research Group from 1993 to 2008 and a long-time friend and colleague working with us in Russia, Scandinavia, the Baltic States, the Alps, and the Andes. Lastly, we could not have completed our joint teamwork in the Western Alps without support: a) from Pierre Tricart (University of Grenoble), who doggedly pursued yearly research permits with the Guil R. Park authority, and b) the invaluable assistance of Professor David Krinsley (deceased, 2017), Department of Geology and CAMCOR, University of Oregon, who vigorously supported the Viso Massif research. We thank Marc Young, Jim Kennett, and other members of the Comet Research Group for constructive discussions of various aspects of the YDIH, including the relevance of Hiawatha Crater to the debate. Of special significance, we thank Marc Young (Flinders University, Australia) for the close editing of this ms. We also acknowledge support from the staff of the CAF Refuge du Viso (France), Refugio Giacoletti, and Refugio Albergo Pian del Re (Italia), Marco Rastelli, Chief Technician, Mon Viso Park Italia, granted permits to work in the upper Po Catchment and ensured we respected endangered species habitat.

Data availability

This research is the product of previous work over several decades, and the data availability resides in the lead author's (WCM) lab files and computer hard drives, accessible to all at any reasonable time. Data related to clast rind and paleosol sediment collected from 2015–2017 reside in files collated by Peeter Somelar, University of Tartu, Department of Geology, Tartu, Estonia.

Declaration of Potential Conflicts

A.W. is a director of the Comet Research Group that funded the publication of this manuscript. W.C.M. and A.W. are on the editorial board of ScienceOpen's journal, Airbursts and Cratering Impacts, but they recused themselves from the editorial process and played no role in reviewing or accepting this contribution. There are no other conflicts of interest to declare, financial or otherwise.

No AI or AI technologies were used in the preparation of this ms.

References

- [1] Mahaney, W.C.; Somelar, P.; Allen, C.C.R. Late Pleistocene Glacial-Paleosol-Cosmic Record of the Viso Massif–France and Italy: New Evidence in Support of the Younger Dryas Boundary (12.8 ka). *Int. J. Earth Sci.* **2022**, *112*(4); doi: 10.1007/s00531.022.02243.9.
- [2] Mahaney, W.C. The Younger Dryas Boundary (YDB): Terrestrial, Cosmic, or Both? *Int. J. Earth Sci.* **2023**, *112*(3), 791–804; doi: 10.1007/s00531.022.02287.x.
- [3] Mahaney, W.C. Paleoenvironmental Archives in Rock Rinds and Sand/Silt Coatings. *J. Geol.* **2019**, *127*, 411–436; doi: 10.1086/703537.
- [4] Mahaney, W.C.; Keiser, L. Weathering Rinds-Unlikely Host Clasts for an Impact-Induced Event. *Geomorphology* **2013**, *184*, 74–83; doi: 10.1016/j.geomorph.2012.11.019.
- [5] Mahaney, W.C.; Dohm, J.M.; Fairen, A. Weathering Rinds on Clasts: Examples from Earth and Mars as Short-and-Long-Term Recorders of Paleoenvironment. *J. Planet. Space Sci.* **2012**, *73*, 243–253; doi: 10.1016/j.pss.2012.08.025.
- [6] Mahaney, W.C.; Keiser, L.; Krinsley, D.H.; Pentlavalli, P.; Allen, C.C.R.; Somelar, P.; Schwartz, S.; Dohm, J.M.; Dirzowsky, R.; West, A.; et al. Weathering Rinds as Mirror Images of Palaeosols: Examples from the Western Alps with Correlation to Antarctica and Mars. *J. Geol. Soc.* **2013**, *170*(5), 833–847; doi: 10.1144/jgs2012.150.
- [7] Mahaney, W.C.; Keiser, L.; Krinsley, D.H.; Kalm, V.; Beukens, R.; West, A. New Evidence from a Black Mat Site in the Northern Andes Supporting a Cosmic Impact 12,800 Years Ago. *J. Geol.* **2013**, *121*(4), 309–325; doi: 10.1086/670652.
- [8] Mahaney, W.C.; Somelar, P.; Dirzowsky, R.W.; Kelleher, B.; Pentlavalli, P.; McLaughlin, S.; Kulakova, A.N.; Jordan, S.; Pulleyblank, C.; West, A.; et al. A Microbial Link to Weathering of Postglacial Rocks and Sediments, Mt. Viso Area, Western Alps, Demonstrated Through Analysis of a Soil/Paleosol Bio/Chronosequence. *J. Geol.* **2016**, *124*, 149–169; doi: 10.1086/684442.
- [9] Mahaney, W.C.; Krinsley, D.H.; Razink, J.; Fischer, R.; Langworthy, K. Clast Rind Analysis Using Multi-High Resolution Instrumentation. *Scanning* **2016**, *38*, 202–212; doi: 10.1002/sca.21255.
- [10] Mahaney, W.C.; Somelar, P.; West, A.; Krinsley, D.H.; Allen, C.C.R.; Pentlavalli, P.; Young, J.M.; Dohm, J.M.; LeCompte, M.; Kelleher, B.; et al. Evidence for Cosmic Airburst/Impact in the Western Alps Archived in Late Glacial Paleosols. *Quat. Int.* **2017**, *438*, 69–80; doi: 10.1016/j.quaint.2017.01.043.
- [11] Mahaney, W.C.; Kalm, V. Late Holocene Paleoclimate and Weathering History in the Norra Storfjället Mountains, Sweden: Solifluction and ¹⁴C Dated Pedostratigraphy. *Geomorphology* **2013**, *173–174*, 43–51.
- [12] Kjær, K.H.; Larsen, N.K.; Binder, T.; Bjørk, A.A.; Eisen, O.; Fahnestock, M.A.; Funder, S.; Garde, A.A.; Haack, H.; Helm, V.; et al. A Large Impact Crater Beneath Hiawatha Glacier in Northwest Greenland. *Sci. Adv.* **2018**, *4*, 8173; doi: 10.1126/sciadv.aar8173.
- [13] Garde, A.A.; Keulen, N.; Waight, T. Microporphyritic and Microspherulitic Melt Grains, Hiawatha Crater, Northwest Greenland: Implications for Post-Impact Cooling Rates, Hydration, and the Cratering Environment. *G.S.A. Bull.* **2022**, *134*(7, 8), 2145–2166; doi: 10.1130/B36058.1.
- [14] Silber, E.A.; Johnson B.C.; Bjonnes, E.; MacGregor, J.A.; Larsen, N.K.; Wiggins, S.E. Effect of Ice Sheet Thickness on Formation of the Hiawatha Impact Crater. *Earth Planet. Sci. Lett.* **2021**, *566*, 116972; doi: 10.1016/j.epsl.2021.116972.
- [15] Kenny, G.G.; William, R.H.; Michael, S.; Adam, A.G.; Martin, J.W.; Pierre, B.; Leif, J.; Søndergaard, A.S.; Bjørk, A.A.; MacGregor, J.A.; et al. A Late Paleocene age for Greenland's Hiawatha Impact Structure. *Sci. Adv.* **2022**, *8*(10), eabm2434; doi: 10.1126/sciadv.abm2434.
- [16] Hyde, W.R.; Larsen, N.K.; Kenny, G.G.; Whitehouse, M.J. U-Pb Analyses of Neoblastic and Porous Monazite Reveal Target Rock and Impact Ages at the Hiawatha Impact Structure, Greenland. In 85th Annual Meeting of the Meteoritical Society, August 2022; Glasgow, Scotland, 2022.
- [17] Dohm, J.M.; Fink, W.; Williams, J.-P.; Mahaney, W.C.; Ferris, J.C. Gale Impact Into ~Half Ocean and Half Land: Martian Chicxulub Analogue. *Icarus* **2022**, *390*, 115306; doi: 10.1016/j.icarus.2022.115306.
- [18] Firestone, R.B.; West, A.; Kennett, J.P.; Becker, L.; Bunch, T.E.; Revay, Z.; Schultz, P.H.; Belgya, T.; Kennett, D.J.; Erlanson, J.M.; et al. Evidence for an Extraterrestrial Impact 12,900 Years ago that Contributed to the Megafaunal Extinctions and the Younger Dryas Cooling. *Proc. Natl. Acad. Sci. U. S. A.* **2007**, *104*, 16016–16021; doi: 10.1073/pnas.0706977104.
- [19] Firestone, R.B.; West, A.; Revay, Z.; Belgya, T.; Smith, A.; Que Hee, S.S. Evidence for a Massive Extraterrestrial Airburst Over North America 12.9 ka Ago. American Geophysical Union Mtg. 07, PP41A Sessions, San Francisco, AGU Annual Mtg. 2007; pp. PP41A–02.
- [20] Hyde, W.R.; Kenny, G.G.; Whitehouse, M.J.K.; Wirth, R.; Roddatis, R.; Schreiber, A.; Adam, A.; Garde, A.A.; Plan, A.; Nicolaj, K.; et al. Microstructural and Isotopic analysis of Shocked Monazite from the Hiawatha Impact Structure: Development of Porosity and its Utility in Dating Impact Craters. *Contrib. Mineral. Petrol.* **2024**, *179*, 28; doi: 10.1007/s00410.024.02097.1.
- [21] Napier, W.M. Palaeolithic Extinctions and the Taurid Complex. *Monthly Notes Royal. Astron. Soc.* **2010**, *405*, 1901–1906; doi: 10.1111/j.1365.2966.2010.16579.x.
- [22] Napier, W.M. The Hazard from Fragmenting Comets. *Mon. Not. R. Astron. Soc.* **2019**, *488*, 1822–1827; doi: 10.1093/mnras/stz1769.
- [23] Teller, J.T.; Leverington, D.W.; Mann, J.D. Freshwater Outbursts to the Oceans from Glacial Lake Agassiz and their Role in Climate Change During the Last Deglaciation. *Quatern Sci. Rev.* **2002**, *21*, 879–887; doi: 10.1016/S0277.3791(01)00145.7.
- [24] Petaev, M.I.; Huang, S.; Jacobsen, S.B.; Zindler, A. Large Pt Anomaly in the Greenland Ice Core Points to a Cataclysm at the Onset of Younger Dryas. *Proc. Natl. Acad. Sci. U. S. A.* **2013**, *110*(32), 12917–12920; doi: 10.1073/pnas.1303924110.
- [25] Firestone, R.B.; West, A.; Revay, Z.; Hagstrum, J.T.; Belgya, T.; Que Hee, S.S.; Smith, A.R. Analysis of the Younger Dryas Impact Layer. *J. Sib. Fed. Univ. Eng. Techn.* **2010**, *3*, 30–62.
- [26] Pino, M.; Abarzúa, A.M.; Astorga, G.; Martel-Cea, A.; Cossio-Montecinos, N.; Navarro, R.X.; Lira M.P.; Labarca R.; LeCompte M.A.; Adedeji V.; et al. Sedimentary Record from Patagonia, Southern Chile Supports Cosmic-Impact Triggering of Biomass Burning, Climate Change, and Megafaunal Extinctions at 12.8 ka. *Sci. Rep.* **2019**, *9*(1), 4413; doi: 10.1038/s41598.018.38089.y.
- [27] Moore, C.R.; Brooks, M.J.; Dunbar, J.S.; Hemmings, C.A.; Langworthy, K.A.; West, A.; LeCompte, M.A.; Adedeji, V.; Kennett, J.P.; Feathers, J.K. Platinum and Microspherule Peaks as Chronostratigraphic Markers for Onset of the Younger Dryas at Wakulla Springs, Florida. *Sci. Rep.* **2023**, *13*, 22738; doi: 10.1038/s41598.023.50074.8.
- [28] Kinzie, C.R.; Que Hee, S.S.; Stich, A.; Tague, K.A.; Mercer, C.; Razink, J.J.; Kennett, D.J.; DeCarli, P.S.; Bunch, T.E.; Wittke, J.H. Nanodiamond-rich Layer Across Three Continents Consistent with Major Cosmic Impact at 12,800 cal BP. *J. Geol.* **2014**, *122*(5), 475–506.
- [29] Moore, A.M.T.; Kennett, J.P.; Napier, W.M.; Bunch, T.E.; Weaver, J.C.; LeCompte, M.; Adedeji, A.V.; Hackley, P.; Kletetschka, G.; Hermes, R.E.; et al. Evidence of Cosmic Impact at Abu Hureyra, Syria at the Younger Dryas Onset (~128 ka): High-Temperature Melting at >2200 °C. *Sci. Rep.* **2020**, *10*, 4185. 10.1038/s41598.020.60867.
- [30] Moore, A.M.T.; Kennett, J.P.; LeCompte, M.; Moore, C.R.; Li, Y.-Q.; Kletetschka, G.K.; Langworthy, K.; Razink, J.J.; Brogden, V.; van Deventer, B.; et al. Abu Hureyra, Syria, Part 1: Shock-Fractured Quartz Grains Support 12,800-Year-Old Cosmic Airburst at the Younger Dryas Onset. *ScienceOpen* **2023**, *1*, 1–28.

- [31] Moore, A.M.T.; Kennett, J.P.; Napier, W.M.; Bunch, T.E.; Weaver, J.C.; LeCompte, M.A.; Adedeji, A.V.; Kletetschka, G.; Hermes, R.E.; Wittke, J.H.; et al. Abu Hureyra, Syria, Part 2: Additional Evidence Supporting the Catastrophic Destruction of this Prehistoric Village by a Cosmic Airburst ~12,800 Years Ago. *ScienceOpen* **2023**, *1*, 1–36.
- [32] Moore, A.M.T.; Kennett, J.P.; Napier, W.M.; LeCompte, M.A.; Moore, C.R.; West, A. Abu Hureyra, Syria, Part 3: Comet Airbursts Triggered Major Climate Change 12,800 Years Ago that Initiated the Transition to Agriculture. *ScienceOpen* **2023**, *1*, 1–24.
- [33] Thackeray, J.F.; Scott, L.; Pieterse, P. The Younger Dryas Interval at Wonderkrater (South Africa) in the Context of a Platinum Anomaly. *Palaeontol. Africa* **2019**, *54*, 30–35; doi: 10.5067/ASTER/ASTGTM.002.
- [34] Mahaney, W.C.; Krinsley, D.H.; Milner, M.W.; Langworthy, K.; Fischer, R. Did the Black Mat/Airburst Reach the Antarctic? Evidence from New Mountain near the Taylor Glacier in the Dry Valleys. *J. Geol.* **2018**, *126*, 285–305.
- [35] Teller, J.T.; Boyd, M.; LeCompte, M.; Kennett, J.; West, A.; Telka, A.; Diaz, A.; Adedeji, V.; Batchelor, D.; Mooney, C.; et al. A Multi-Proxym Study of Changing Environmental Conditions in a Younger Dryas Sequence in Southwestern Manitoba, Canada, and Evidence for an Extraterrestrial Event. *Quat. Res.* **2020**, *93*, 60–87; doi: 10.1017/qua.2019.46.
- [36] Lowe, J.J.; Rasmussen, S.O.; Björck, S.; Hoek, W.Z.; Steffensen, J.P.; Walker, M.J.C.; Yu, Z.C. Synchronisation of Palaeoenvironmental Events in the North Atlantic Region During the Last Termination: A Revised Protocol Recommended by the INTIMATE Group. *Quat. Sci. Rev.* **2008**, *27*, 6–17; doi: 10.1016/j.quascirev.2007.09.016.
- [37] Hartz, N.; Milthers, V. Det sennglaciale Ler i Allerød Teglværksgrav. *Meddelelser fra Dansk geologisk Forening* **1901**, *8*, 31–60.
- [38] Hartz, N. Allerød-Gytje und Allerød-Mull. *Meddelelser fra Dansk Geologisk Forening* **1912**, *4*, 85–91.
- [39] Mangerud, J. The Discovery of the Younger Dryas, and Comments on the Current Meaning and Usage of the Term. *Boreas* **2021**, *50*, 1–5; doi: 10.1111/bor.12481.
- [40] Israde-Alcántara, I.; Bischoff, J.L.; Domínguez-Vázquez, G.; Li, H.-C.; DeCarli, P.S.; Bunch, T.E.; Wittke, J.H.; Weaver, J.C.; Firestone, R.B.; West, A.; et al. Evidence from Central Mexico Supporting the Younger Dryas Extraterrestrial Impact Hypothesis. *Proc. Natl. Acad. Sci. U. S. A.* **2012**, *109*, E738–E747; doi: 10.1073/pnas.1110614109.
- [41] Ge, T.; Courty, M.M.; Guichard, F. Field-Analytical Approach of Land-Sea Records for Elucidating the Younger Dryas Boundary Syndrome. *American Geophysical Union* **2009**, *432*, Abstract PP31D-1390.
- [42] LeCompte, M.; Goodyear, A.C.; Demitroff, M.N.; Batchelor, D.; Vogel, E.K.; Mooney, C.; Rock, B.N.; Seidel, A.W. An Independent Evaluation of Conflicting Microspherule Results from Different Investigations of the Younger Dryas Impact Hypothesis. *Proc. Natl. Acad. Sci. USA* **2012**, *106*(44), E2960–E2969; doi: 10.1073/pnas.1208603109.
- [43] Andronikov, A.V.; Van Hoesel, A.; Andronikova, I.E.; Hoek, W.Z. Trace Element Distribution and Implications in Sediments Across the Allerød – Younger Dryas Boundary in the Netherlands and Belgium. *Geogr. Ann. Ser. B* **2016**, *98*, 325–345; doi: 10.1111/geoa.12140.
- [44] Wittke, J.H.; Weaver, J.C.; Bunch, T.E.; Kennett, J.P.; Kennett, D.J.; Moore, A.M.T.; Hillman, G.C.; Tankersley, K.B.; Goodyear, A.C.; Moore, C.R.; et al. Evidence for Deposition of 10 Million Tonnes of Impact Spherules Across Four Continents 12,800 Years Ago. *Proc. Natl. Acad. Sci. U. S. A.* **2013**, *110*(23), E2088–E2097; doi: 10.1073/pnas.1301760110.
- [45] Kennett, D.J.; Kennett, J.P.; West, A.; Mercer, C.; Que Hee, S.S.; Bement, L.; Bunch, T.E.; Sellers, M.; Wolbach, W.S. Nanodiamonds in the Younger Dryas Boundary Sediment. *Science* **2009**, *323*(5910), 94; doi: 10.1126/science.1162819.
- [46] Kennett, J.P.; Kennett, D.J.; Culleton, B.J.; Tortosa, J.E.A.; Bischoff, J.L.; Bunch, T.E.; Daniel, I.R.; Erlandson, J.M.; Ferraro, D.; Firestone, R.; et al. Bayesian Chronological Analyses Consistent with Synchronous Age of 12835–12735 Cal BP for Younger Dryas Boundary on Four Continents. *Proc. Natl. Acad. Sci.* **2015**, *2*, 2. 10.1073/pnas.1507146112.
- [47] Lohne, Ø.S.; Mangerud, J.; Birks, H.H. Precise C14 Ages of the Vedde and Saksunarvatn Ashes and the Younger Dryas Boundaries from Western Norway and their Comparison with the Greenland Ice Core (GICC05) Chronology. *J. Quat. Sci.* **2013**, *2*, 490–500; doi: 10.1002/jqs.2640.
- [48] Lohne, Ø.S.; Mangerud, J.; Birks, H.H. IntCal13 Calibrated Ages of the Vedde and Saksunarvatn Ashes and the Younger Dryas Boundaries from Krakenes, Western Norway. *J. Quat. Sci.* **2014**, *29*, 506–507; doi: 10.1002/jqs.2722.
- [49] Engels, S.; Lane, C.S.; Haliuc, A.; Hoek, W.Z.; Muschitiello, F.; Baneschi, I.; Bouwman, A.; Bronk Ramsey, C.; Collins, J.; de Bruijn, R.; et al. Synchronous Vegetation Response to the Last Glacial-Interglacial Transition in Northwest Europe. *Nat. Commun. Earth Environ.* **2022**, *3*(1), 130; doi: 10.1038/s43247.022.00457.y.
- [50] Lyell, C. Principles of Geology-3 Volumes; London: John Murray, 1830-33.
- [51] Bunch, T.E.; Hermes, R.E.; Moore, A.M.T.; Kennett, D.J.; Weaver, J.C.; Wittke, J.H.; DeCarli, P.S.; Bischoff, J.L.; Hillman, G.C.; Howard, G.A.; et al. Very High-Temperature Impact Melt Products as Evidence for Cosmic Airbursts and Impacts 12,900 Years Ago. *Proc. Natl. Acad. Sci. U. S. A.* **2012**, *109*(28), E1903–E1912; doi: 10.1073/pnas.1204453109.
- [52] Bunch, T.E.; LeCompte, M.A.; Victor Adedeji, A.; Wittke, J.H.; David Burleigh, T.; Hermes, R.E.; Mooney, C.; Batchelor, D.; Wolbach, W.S.; Kathan, J.; et al. A Tunguska-sized Airburst Destroyed Tall el-Ham-mam a Middle Bronze Age City in the Jordan Valley near the Dead Sea. *Sci. Rep.* **2021**, *11*(1), 1–64; doi: 10.1038/s41598.021.97778.3.
- [53] Shoemaker, E.M. Impact Mechanics at Meteor Crater, Arizona, Ph.D. Thesis. Princeton, NJ: Princeton University, 1959; pp. 55.
- [54] Hermes, R.E.; Wenk, H.-R.; Kennett, J.P.; Bunch, T.E.; Moore, C.R.; LeCompte, M.A.; Kletetschka, G.; Victor Adedeji, A.; Langworthy, K.; Razink, J.J.; et al. Microstructures in Shocked Quartz: Linking Nuclear Airbursts and Meteorite Impacts. *Airburs. Crater. Imp.* **2023**, *1*(1), 1–40; doi: 10.14293/ACI.2023.0001.
- [55] Svetsov, V. Total Ablation of the Debris from the 1908 Tunguska Explosion. *Nature* **1996**, *383*, 697–699; doi: 10.1038/383697a0.
- [56] De Pater, L.; Lissaur, J. Planetary Sciences; Cambridge University Press, 2001. ISBN 0521482194.
- [57] Turco, R.P.; Toon, O.B.; Park, C.; Whitten, R.C.; Pollack, J.B.; Noerdlinger, P. An Analysis of the Physical, Chemical, Optical and Historical Impacts of the 1908 Tunguska Meteor Fall. *Icarus* **1982**, *50*(1), 1–52; doi: 10.1016/0019.1035(82)90096.3.
- [58] Moore, C.R.; LeCompte, M.A.; Kennett, J.P.; Brooks, M.J.; Firestone, R.B.; Ivester, A.H.; Ferguson, T.A.; Lane, C.S.; Duernberger, K.A.; Feathers, J.K.; et al. Platinum, Shock-Fractured Quartz, Microspherules, and Meltglass Widely Distributed in Eastern USA at the Younger Dryas Onset (12.8 ka). *Airburs. Crater. Imp.* **2024**, *2*.
- [59] Deer, W.A.; Howie, R.A.; Zussman, J. An Introduction to the Rock-Forming Minerals; Wiley: New York, 1966, pp. 340–355. ISBN0-582-44210-9.
- [60] Schwartz, S.; Lardeaux, J.M.; Guillot, S.; Tricart, P. The Diversity of Eclogitic Metamorphism in the Monviso Ophiolitic Complex, Western Alps, Italy. *Geodin Acta.* **2000**, *13*, 169–188.
- [61] NSSC (National Soil Survey Center). Soil Survey Laboratory Information Manual. Soil Survey Investig. Rep. 45, version 1.00; US Department of Agriculture: Lincoln, NE, 1995, pp. 305.
- [62] Birkeland, P.W. Soils and Geomorphology; Oxford University Press: Oxford, 1999; pp. 430.
- [63] Hodgson, J.M. Soil Survey Field Handbook, Soil Survey Tech. Monograph No. 5. Rothamsted Experimental Station: Harpenden, Herts, UK, 1976; pp. 99.

- [64] Canada Soil Survey Committee. The Canadian System of Soil Classification; 637 NRC Research Press (publ. 1646): Ottawa, 1998; pp. 187.
- [65] Oyama, M.; Takehara, H. Standard Soil Color Charts; Japan Research Council for Agriculture, Forestry and Fisheries: Tokyo, Japan, 1970.
- [66] Rudnick, R.L.; Gao, S. Composition of the Continental Crust. In The Crust: Treatise on Geochemistry; Rudnick R.L., Ed.; Elsevier: Amsterdam, 2005; pp. 1–64.
- [67] Wang, X.S.; Sun, C. Pt and Pd Concentrations and Source in Urban Roadside Soils from Xuzhou, China. *Environ. Geol.* **2008**, *56*, 1129–1133; doi: 10.1007/s00254-008-1213-4.
- [68] Young, J.M.; Skvortsov, T.; Kelleher, B.P.; Mahaney, W.C.; Somelar, P.; Allen, C.C.R. Effect of Soil Horizon Stratigraphy on the Microbial Ecology of Alpine Paleosols. *J. Total Environ.* **2018**, *657*, 1183–1193; doi: 10.1016/j.scitotenv.2018.11.442.
- [69] Wolbach W.S.; Ballard, J.P.; Mayewski, P.A.; Parnell, A.C.; Cahill, N.; Adedeji, V.; Bunch, T.E.; Domínguez-Vázquez, G.; Erlandson, J.M.; Firestone, R.B.; et al. Extraordinary Biomass-Burning Episode and Impact Winter Triggered by the Younger Dryas Cosmic Impact ~12,800 Years Ago. 1. Ice Cores and Glaciers. *J. Geol.* **2018**, *126*(2), 165–184; doi: 10.1086/695703.
- [70] Wolbach W.S.; Ballard, J.P.; Mayewski, P.A.; Parnell, A.C.; Cahill, N.; Adedeji, V.; Bunch, T.E.; Domínguez-Vázquez, G.; Erlandson, J.M.; Firestone, R.B.; et al. Extraordinary Biomass-Burning Episode and Impact Winter Triggered by the Younger Dryas Cosmic Impact ~12,800 Years Ago. 2. Lake, Marine, and Terrestrial Sediments. *J. Geol.* **2018**, *126*(2), 185–205; doi: 10.1086/695704.
- [71] Van Ginneken, M.; Goderis, S.; Artemieva, N.; Debaille, V.; Decree, S.; Harvey, R.P.; Huwig, K.A.; Hechet, L.; Yang, S.; Kaufmann, F.E.D.; et al. A Large Meteoritic Event Over Antarctica ca. 430 ka Ago Inferred from Chondritic Spherules from the Sør Rondane Mountains. *Sci. Adv.* **2021**, *7*(14), eabc1008. doi: 10.1126/sciadv.abc1008.
- [72] Van Ginneken, M.; Harvey, R.P.; Goderis, S.; Artemieva, N.; Boslough, M.; Maeda, R.; Gattacceca, J.; Folco, L.; Yamaguchi, A.; Sonzogni, C.; et al. The Identification of Airbursts in the Past: Insights from the BIT-58 Layer. *Earth Planet. Sci. Lett.* **2024**, *627*, 118562; doi: 10.1016/j.epsl.2023.118562.
- [73] Hattori, K. H.; Guillot, S. Geochemical Character of Serpentinites Associated with High- to Ultrahigh-Pressure Metamorphic Rocks in the Alps, Cuba, and the Himalayas: Recycling of Elements in Subduction Zones. *Geochem. Geophys. Geosyst.* **2007**, *8*, Q09010; doi: 10.1029/2007GC001594.
- [74] Quesnel, F., Prost, A.E.; Lablanche, G.; Thiry, M.; Simon-Coinçon, R. Carte géologique de la France à 1/50 000, feuille 595, Châteaumeillant, January 2006 Edition, Bureau de Recherches géologiques et Minières (BRGM), Orléans, 2006. ISBN: 978-2-7259-1595-4.
- [75] Wolbach, W.S.; Ballard, J.P.; Bunch, T.E.; LeCompte, M.A.; Adedeji, V.; Firestone, R.B.; Mahaney, W.C.; Melott, A.I.; Moore, C.R.; Napier, W.M.; et al. Extraordinary Biomass-Burning Episode and Impact Winter Triggered by the Younger Dryas Cosmic Impact ~12,800 Years Ago: A Reply. *J. Geol.* **2019**, *128*(1), 95–107; doi: 10.1086/706265.